High receiver responsivity and low dark current of InP-based pin-photodiode array monolithically integrated with 90° hybrid and spot-size converter using selective embedding regrowth

Hideki Yagi[a]), Naoko Inoue, Takehiko Kikuchi, Ryuji Masuyama, Tomokazu Katsuyama, Yoshihiro Tateiwa, Katsumi Uesaka, Yoshihiro Yoneda, Masaru Takechi, and Hajime Shoji

Transmission Devices R & D Laboratories, Sumitomo Electric Industries, LTD.,
1 Taya-cho, Sakae-ku, Yokohama 244–8588, Japan
a) *yagi-hideki@sei.co.jp*

Abstract: The InP-based pin-photodiode array monolithically integrated with a 90° hybrid and spot-size converters was realized using selective embedding regrowth for compact 100 Gb/s coherent receivers. The low dark current of less than 500 pA up to 85 °C was attained by InP passivation effect in four-channel pin-photodiodes. As a receiver using these photodiode arrays, a receiver responsivity including total loss of 6.7 dB in the 90° hybrid and intrinsic loss of 3 dB in the polarization beam splitter was higher than 0.060 A/W between −5 °C and 85 °C through the integration of the spot-size converter. Responsivity imbalance of the In-phase and Quadrature channels was also less than 0.5 dB over the C-band.

Keywords: coherent transmission, 90° hybrid, multimode interference structure, pin-photodiode, butt-joint regrowth, selective embedding regrowth

Classification: Optoelectronics, Lasers and quantum electronics, Ultrafast optics, Silicon photonics, Planar lightwave circuits

References

[1] S. Tsukamoto, D.-S. Ly-Gagnon, K. Katoh and K. Kikuchi: Proc. OFC/NFOEC 2005 (2005) paper PDP29. DOI:10.1109/OFC.2005.193207

[2] R. Noe: J. Lightwave Technol. **23** (2005) 802. DOI:10.1109/JLT.2004.838818

[3] G. Charlet, J. Renaudier, H. Mardoyan, P. Tran, O. Bertran Pardo, F. Verluise, M. Achouche, A. Boutin, F. Blache, J.-Y. Dupuy and S. Bigo: Proc. OFC/NFOEC 2008 (2008) paper PDP3.

[4] S. Oda, T. Tanimura, T. Hoshida, C. Ohshima, H. Nakashima, Z. Tao and J. C.

Rasmussen: Proc. OFC/NFOEC 2009 (2009) paper OThR6.

[5] H.-G. Bach, A. Matiss, C. C. Leonhardt, R. Kunkel, D. Schmidt, M. Schell and A. Umbach: Proc. OFC/NFOEC 2009 (2009) paper OMK5.

[6] C. R. Doerr, P. J. Winzer, S. Chandrasekhar, M. Rasras, M. Earnshaw, J. Weiner, D. M. Gill and Y. K. Chan: Proc. OFC/NFOEC 2009 (2009) paper PDPB2.

[7] V. Houtsma, N. G. Weimann, T. Hu, R. Kopf, A. Tate, J. Frackoviak, R. Reyes, Y. K. Chen, L. Zhang, C. R. Doerr and D. T. Neilson: Proc. OFC/NFOEC 2011 (2011) paper OML2.

[8] Y. Painchaud, M. Pelletier, M. Poulin, F. Pelletier, C. Latrasse, G. Robidoux, S. Savard, J.-F. Gagne, V. Trudel, M.-J. Picard, P. Poulin, P. Sirois, F. D' Amours, D. Asselin, S. Paquet, C. Paquet, M. Cyr, M. Guy, M. Morsy-Osman, Q. Zhuge, X. Xu, M. Chagnon and D. V. Plant: Proc. OFC/NFOEC 2013 (2013) paper OM2J.2.

[9] M. Itoh and Y. Kurata: Proc. OFC/NFOEC 2013 (2013) paper OTh3H.4.

[10] P. Runge, S. Schubert, A. Seeger, K. Janiak, J. Stephan, D. Trommer and A. Matiss: Proc. European Conference and Exhibition on Optical Communication (ECOC) 2012 (2012) paper Mo.2.E.3.

[11] H. Yagi, N. Inoue, Y. Onishi, R. Masuyama, T. Katsuyama, T. Kikuchi, Y. Yoneda and H. Shoji: Proc. OFC/NFOEC 2013 (2013) paper OW3J.5.

[12] S.-H. Jeong and K. Morito: Proc. European Conference and Exhibition on Optical Communication (ECOC) 2009 (2009) paper 2.2.3.

[13] R. Masuyama, H. Yagi, N. Inoue, Y. Onishi, T. Katsuyama, T. Kikuchi, Y. Yoneda and H. Shoji: Proc. Indium Phosphide and Related Materials (IPRM) 2013 (2013) paper MoD3-6. DOI:10.1109/ICIPRM.2013.6562573

[14] H. Yagi, Y. Yoneda, M. Takechi and H. Shoji: Proc. Conference on Lasers and Electro-optics (CLEO) 2014 (2014) paper STu1G.3.

[15] M. Takechi, Y. Tateiwa and S. Ogita: Proc. European Conference and Exhibition on Optical Communication (ECOC) 2013 (2013) paper P.2.8.

1   Introduction

The coherent transmission technology with digital signal processing (DSP) for multi-level modulation formats such as quadrature phase-shift keying (QPSK) and quadrature amplitude modulation (QAM) is very attractive for 100 Gb/s long-haul networks, because it has a high receiver sensitivity and high resilience to linear impairments such as chromatic dispersion and polarization mode dispersion [1, 2, 3, 4]. Currently, application to not only long-haul networks but also metro networks has been expected in this transmission technology, and high port density with downsizing of optical components including a coherent receiver is strongly required for metro applications.

InP-based photodiodes monolithically integrated with a 90° hybrid for a coherent receiver have some advantages over other approaches, since they can offer a smaller footprint in packaging and eliminate complicated alignments in the assembly process. Consequently, they bring about low production costs and stabilization of receiver performance with mature process technologies [5, 6, 7, 8, 9]. In addition, the monolithic integration of the 90° hybrid and photodiodes using butt-joint (BJ) regrowth demonstrated high responsivity operation due to lower optical coupling loss for the BJ coupling structure with the direct connection of the

core layer for waveguides from the 90° hybrid and the absorption layer for photo-diodes compared with that for the evanescent coupling structure using the single-step organometallic vapor-phase-epitaxial (OMVPE) growth process [10, 11].

High optical coupling efficiency between the polarization beam splitter (PBS) and the InP-based 90° hybrid is critical in order to achieve a high responsivity of a coherent receiver. The monolithic integration of a spot-size converter (SSC) is very effective for optical coupling with different mode field diameters between PBS and 90° hybrids without a complicated optical configuration.

In this letter, we report a high receiver responsivity and low dark current for the InP-based pin-photodiode array monolithically integrated with a 90° hybrid and SSC by using selective embedding regrowth for compact 100 Gb/s coherent receivers.

2 Device design and fabrication process

Fig. 1 shows (a) the photomicrograph, (b) schematic cross-sectional views of SSC, 90° hybrid and photodiode sections and (c) the schematic diagram of the 90° hybrid for an InP-based pin-photodiode array monolithically integrated with the 90° hybrid and SSC. The chip size was 4.1 mm × 1.6 mm. SSC consisting of a buried heterostructure (BH) was integrated at two optical input ports of the 90° hybrid for achieving high optical coupling efficiency between PBS and 90° hybrids. The 90° hybrid consisting of deep-ridge waveguides has the 2 × 4 multimode interference structure (MMI) working as a 180° hybrid for in-phase relation and 2 × 2 MMI working for quadrature phase relation. Accordingly, the output channels
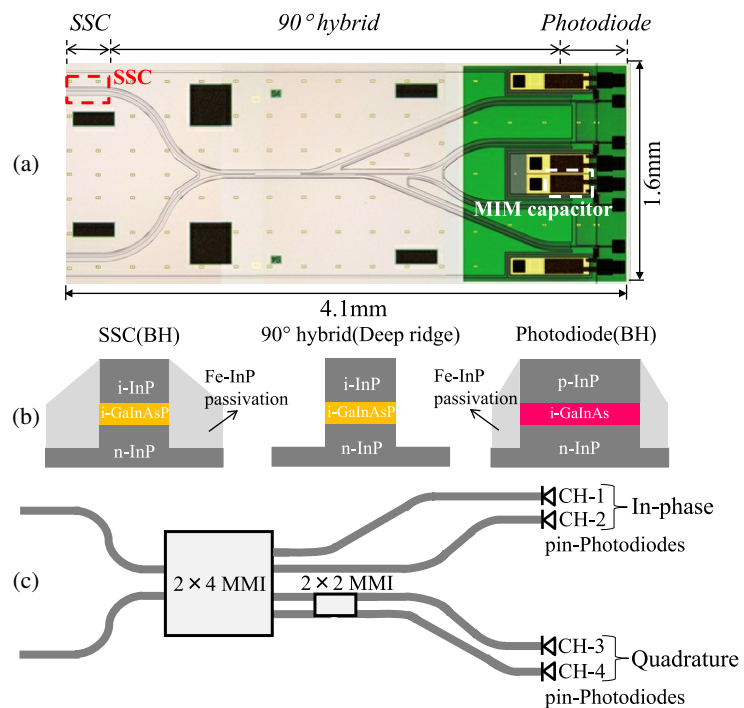

Fig. 1. (a) Photomicrograph, (b) schematic cross-sectional views of SSC, 90° hybrid and photodiode sections and (c) schematic diagram of the 90° hybrid for the InP-based pin-photodiode array monolithically integrated with the 90° hybrid and SSC.

from the 90° hybrid can be directly connected to photodiodes without waveguide intersections which cause excess loss, because the In-phase channels (CH-1 and CH-2) and the Quadrature channels (CH-3 and CH-4) are not spatially separated in this 90° hybrid structure [12]. The waveguide layout and intervals of the In-phase and Quadrature channels were designed by considering the reduction of skew in the 90° hybrid and assembly of trans-impedance amplifiers (TIAs), respectively. Metal-insulator-metal (MIM) capacitors were also monolithically integrated with the photodiode array for downsizing of receiver modules [13].
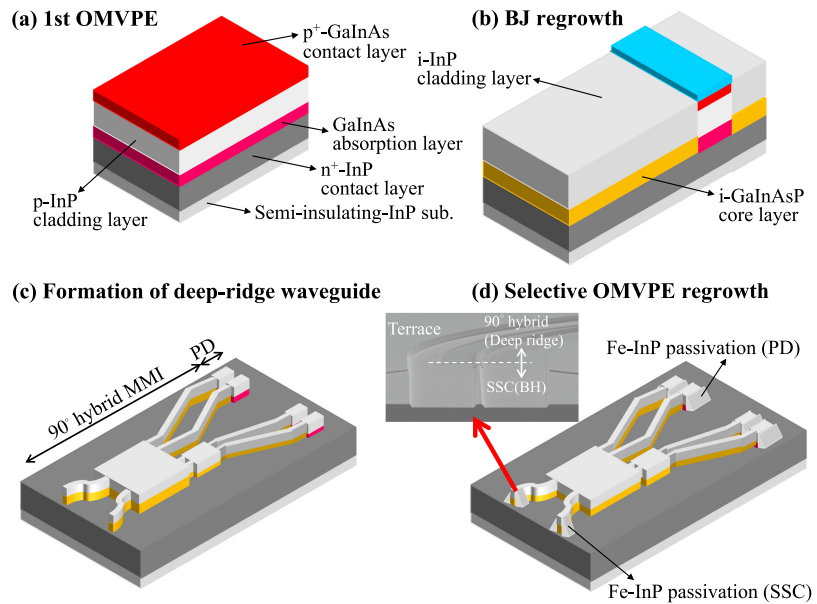

Fig. 2. Fabrication process of the InP-based pin-photodiode array monolithically integrated with the 90° hybrid and SSC. The scanning electron microscope (SEM) image of the SSC section is also indicated in the inset of Fig. 2(d).

Fig. 2 shows the fabrication process of this integrated device. A pin-photodiode structure with a GaInAs absorption layer was prepared on a semi-insulating 3-inch InP wafer by OMVPE growth [Fig. 2(a)]. The waveguide section with the GaInAsP core layer and the photodiode section were combined using the BJ regrowth process [Fig. 2(b)]. Deep-ridge waveguide stripes for SSC, 90° hybrid and photo-diode sections were simultaneously formed by standard optical i-line stepper lithography and reactive ion etching (RIE) techniques [Fig. 2(c)]. BH layers were selectively formed in photodiode sections to reduce the dark current and in SSC sections using OMVPE regrowth techniques [Fig. 2(d)]. Although relatively thin InP passivation was adopted in the photodiode section to suppress parasitic capacitance for a high-speed response, thicker InP passivation was formed in the SSC section to obtain the target mode field diameter (MFD), that is, the wider selective regrowth mask compared with that of the photodiode section was arranged on the terrace part in the side of the SSC waveguide. In the 90° hybrid consisting of MMIs, the deep-ridge waveguide without the InP regrowth was maintained for the reduction of wavelength dependence of loss and for precise phase control. As a result, the pin-photodiode array monolithically integrated with the 90° hybrid and

SSC was realized through the simple fabrication process with the selective regrowth technique. Then, electrodes were evaporated for the p- and n-side ohmic contacts, followed by an anti-reflection (AR) coating on the optical input facet.

3   Measurement results

Fig. 3 shows the temperature dependence of the dark current for four-channel photodiodes integrated with the 90° hybrid at a reverse bias voltage of 3.0 V. The dark current of less than 5.0 pA was obtained at a temperature of 25 °C, and the low dark current of less than 500 pA was attained even at a temperature of 85 °C. Hence, the surface recombination at the sidewall of the deep-ridge stripe in the photodiode section was reduced by passivation effect with the InP regrowth process. Furthermore, the dark current was reduced to 1/10 of the previous structure with undoped InP passivation [14]. It is attributed to the reduction of the leakage current at the interface of the deep-ridge stripe and the BH layer by using Fe-doped InP passivation in the photodiode section.
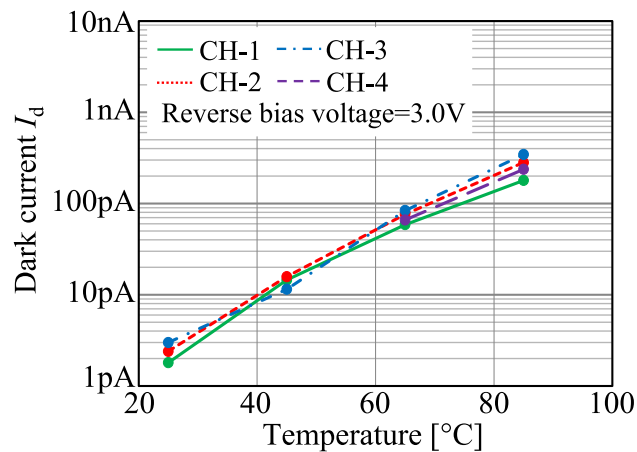

Fig. 3.   Temperature dependence of the dark current for four-channel photodiodes integrated with the 90° hybrid at a reverse bias voltage of 3.0 V.

Fig. 4 shows (a) the photograph and (b) the schematic diagram for a fabricated polarization and phase diversity intradyne coherent receiver. The package body size was 15 mm × 26 mm × 5.5 mm. This receiver was comprised of a beam splitter (BS), PBS, two InP-based pin-photodiode arrays monolithically integrated with the 90° hybrid for transverse electric (TE) polarized light (X-polarization) and transverse magnetic (TM) polarized light (Y-polarization) and four TIAs in one package [15]. The signal light with arbitrary polarization is introduced to the receiver using a single mode fiber (SMF). The signal light from SMF is coupled to the collimate lens. Then, a small portion of the signal light is split to the monitor photodiode (MPD) with BS. At PBS, the signal light is decomposed to TE polarized light and TM polarized light. The TE polarized light is coupled to the InP-based 90° hybrid for X-polarization through the lens. The TM polarized light is converted to TE polarized light with the half-wave plate (HWP). Then, this TE polarized light is coupled to the InP-based 90° hybrid for Y-polarization through the lens.

The local oscillator (LO) light is also introduced to the receiver using a polarization maintaining fiber (PMF). The LO light from PMF is coupled to the collimate lens, and this light is split using BS. Finally, the LO light is coupled to the InP-based 90° hybrid for X-polarization and that for Y-polarization through the lens. Demodulation properties of 128 Gb/s dual polarization quadrature phase-shift keying (DP-QPSK) modulated signals have already been proved in this coherent receiver using InP-based pin-photodiode arrays integrated with the 90° hybrid [14].
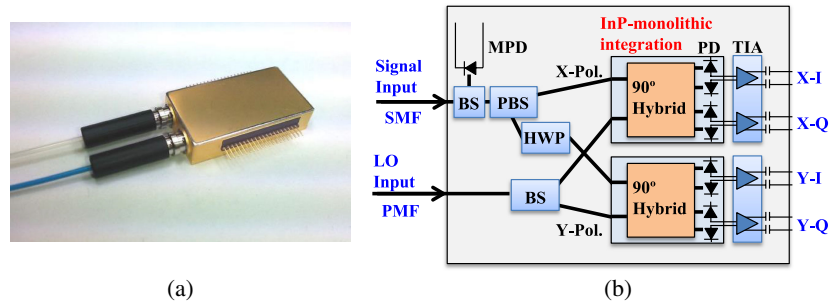

(a)   (b)

Fig. 4. (a) Photograph and (b) schematic diagram for the coherent receiver using InP-based pin-photodiode arrays monolithically integrated with the 90° hybrid and SSC.
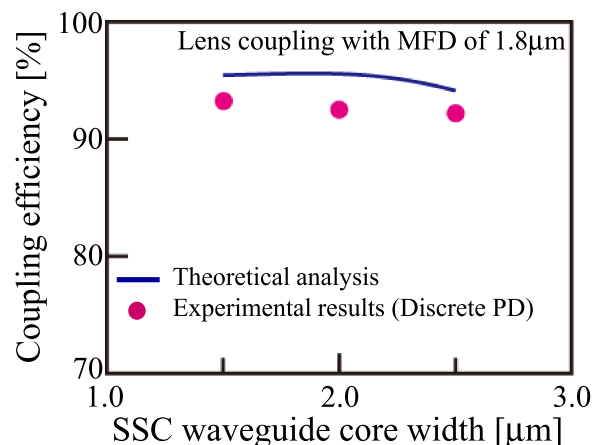

Fig. 5. SSC waveguide core width dependence of optical coupling efficiency. The solid line and circulars indicate the theoretical analysis and experimental results, respectively.

At first, optical coupling efficiency was evaluated using discrete waveguide photodiodes with SSC (total length of photodiode and waveguide sections: 0.9 mm) fabricated on the same wafer with integrated devices. The SSC core width was optimized to obtain high optical coupling efficiency for an optical field consisting of the parallel Gaussian beam in horizontal and vertical directions, which has MFD of 1.8 μm from the optical configuration with lens coupling as shown in Fig. 4(b). This MFD was optimized with vertical MFD which is restricted by the thickness of the upper InP cladding layer for the SSC section. Fig. 5 shows the SSC waveguide core width dependence of optical coupling efficiency. Experimental optical coupling efficiency was larger than 90% for the optical configuration with lens coupling (MFD: 1.8 μm), which had good agreement with the theoretical analysis using the finite element method.

Fig. 6 shows (a) wavelength dependence of the responsivity at a temperature of 25 °C and (b) temperature dependence of the responsivity at a wavelength of 1550 nm for the receiver using two InP-based pin-photodiode arrays integrated with the 90° hybrid and SSC. The receiver responsivity in all channels of 4 channels × 2 devices (device responsivity including hybrid splitting loss of 6.0 dB and propagation loss of 0.7 dB in the 90° hybrid: 0.140 A/W) was higher than 0.060 A/W at a wavelength of 1550 nm with the introduction of SSC, even though the intrinsic loss of 3 dB occurs due to separation of TE polarized light and TM polarized light in PBS. A change of responsivity owing to wavelength dependence of loss for the 90° hybrid consisting of MMIs was also less than 0.6 dB over the C-band. Furthermore, it was stable in a measurement temperature from −5 °C to 85 °C with small wavelength dependence of loss for the 90° hybrid consisting of MMIs as shown in Fig. 6(b). Responsivity imbalance of the In-phase and Quadrature channels was less than 0.5 dB over the C-band through small loss imbalance of the 90° hybrid consisting of 2 × 4 MMI and 2 × 2 MMI. Therefore, the high receiver module responsivity was successfully achieved using the InP-based pin-photodiode array monolithically integrated with the 90° hybrid and SSC.
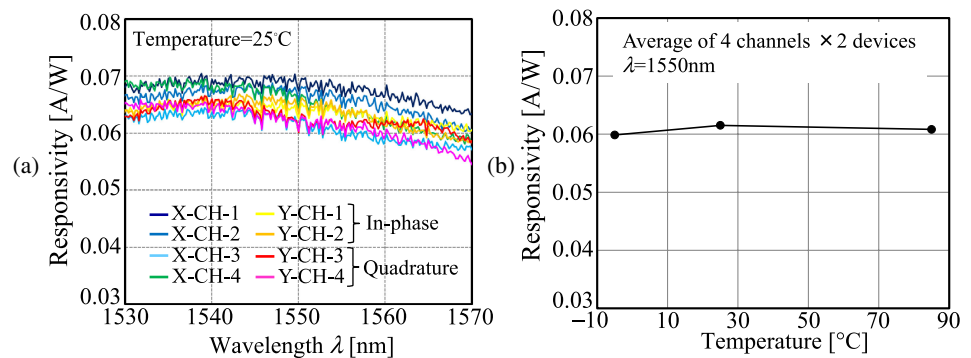

Fig. 6. (a) Wavelength dependence of the responsivity at a temperature of 25 °C and (b) temperature dependence of the responsivity at a wavelength of 1550 nm for the receiver using two InP-based pin-photodiode arrays integrated with the 90° hybrid and SSC.

4 Conclusion

We fabricated the InP-based pin-photodiode array monolithically integrated with the 90° hybrid and spot-size converters. It demonstrated the low dark current (<500 pA @ 85 °C) and the excellent receiver responsivity (>0.060 A/W @ $\lambda =$ 1550 nm) with small imbalance in all channels through the selective regrowth process. From these results, we confirmed that this InP-based monolithically integrated device is very suitable for compact coherent receivers with 100 Gb/s multi-level modulation formats.

Acknowledgments